

Identification of Pressure-Induced Phase Transformations Using Nanoindentation

Vladislav Domnich¹, Yury Gogotsi² and Michael Trenary³

¹Department of Mechanical Engineering, University of Illinois at Chicago,
842 West Taylor Street, Chicago, IL 60607, USA.

²Department of Materials Engineering, Drexel University,
3141 Chestnut Street, Philadelphia, PA 19104, USA.

³Department of Chemistry, University of Illinois at Chicago,
845 West Taylor Street, Chicago, IL 60607, USA.

ABSTRACT

A combination of depth-sensing indentation and Raman microspectroscopy has been used for the identification of pressure-induced phase transformations in silicon, germanium, boron carbide and partially stabilized zirconia single crystals. Phase transformations during nanoindentation may be revealed through deviations in the shape of the load-displacement curves from that of a perfect elastoplastic material. Such deviations are often more readily identified if the nanoindentation data are presented as average contact pressure vs. contact depth curves, allowing assessment of the corresponding transformation pressures.

INTRODUCTION

It is known that the indentation of materials with diamond indenters creates high stresses (hydrostatic and deviatoric) under the indenter that can cause phase transformations [1-4]. It has also been shown that the hardness correlates with metallization pressures for a number of semiconductors [5]. Unfortunately, the successful use of indentation technique to study phase transformations in materials is inhibited by difficulties associated with monitoring the process. Indirect monitoring of phase transformations during indentation through conductivity measurements [1-3, 6] was used in many of the indentation experiments. However, the conductivity measurements can only be used to detect metallic-nonmetallic transitions in materials and the obtained data are significantly affected by a particular experimental setup. Direct studies of the indentations have been conducted using transmission electron microscopy (TEM) [2, 7-9]. However, only amorphous material was repeatedly observed in the residual impressions. Thus, although numerous indirect indications of the structural changes in materials (mostly Si and Ge) during indentation have been observed, direct evidence of the phase transformations was still lacking.

Recent advances in the use of Raman microspectroscopy to study indentation-induced phase transformations in semiconductors and ceramics [10-13] opened new horizons and substantially revived research activity in this area. For example, the most recent, carefully performed TEM experiments [14, 15] indeed revealed metastable high-pressure phases in the residual impressions on Si, confirming the Raman spectroscopy results. Much effort has also been put lately in understanding of the deformation behavior of Si and other semiconductors by combining the depth-sensing indentation data with the new experimental findings of Raman microspectroscopy [16, 17] and TEM [15]. In the present study, we examine the cyclic nanoindentation behavior of several brittle materials in connection with the results of our characterization of the corresponding residual impressions by Raman spectroscopy.

MATERIALS AND EXPERIMENTAL

Four different types of single crystal materials were used in this research. Semiconductor samples included pieces of commercially available polished Si (100) and Ge (100) wafers. Partially stabilized ($\text{ZrO}_2 + 3 \text{ mol.}\% \text{ Y}_2\text{O}_3$) zirconia crystals (PSZ-C) were grown using the skull melting technique. The specimen for nanoindentation experiments was cut out of the PSZ-C and polished using diamond tool; its orientation was determined to be (001) by Laue back reflection method. The boron carbide single crystal was grown using floating zone technique. The crystal composition was determined to be $\text{B}_{4.3}\text{C}$ by analyzing the carbon content. The sample was oriented along (0001) hexagonal direction by Laue back reflection method and then cut and polished using diamond and Al_2O_3 abrasives.

Nanoindentation experiments were performed using a Nano Indenter XP[®] tester (MTS), equipped with a Berkovich pyramidal indenter. The cyclic tests were performed in the following manner: loading to the maximum load and unloading by 90%; reloading to the maximum load and unloading by 95%; hold for 20 s at 5% of the maximum load for thermal drift correction and complete unloading. The maximum loads used were 5, 20, 50, 100, 200, and 300 mN for all materials. The same loading and unloading rates were used, which corresponded to the 100 sec duration of the first loading stage. To reveal possible signs of phase transformations during nanoindentation, the inner load-displacement loops were replotted as average contact pressure vs. contact depth curves following the procedure of Ref. 18.

Raman spectra of the residual impressions were acquired in backscattering geometry using a Ramascope 2000 (Renishaw, UK) Raman microspectrometer equipped with a charge coupled device (CCD) detector. The 514.5 nm excitation line of an Ar ion laser was used. The acquisition times varied from 10 - 60 sec for Si to over 10 min for $\text{B}_{4.3}\text{C}$. Due to the comparable sizes of nanoindentations and the laser probe ($\sim 1 \mu\text{m}$), the Raman spectra in many cases included spectral features of the pristine material outside the indentation contact area.

RESULTS AND DISCUSSION

At quasihydrostatic pressures of 9 to 16 GPa, Si-I (cubic diamond structure) transforms into a $\sim 20\%$ more dense metallic Si-II phase with β -tin structure [19]. On slow decompression, the first phase to form from Si-II at 10-12 GPa is Si-XII or $r8$ (rhombohedral structure with 8 atoms per unit cell), which corresponds to $\sim 9\%$ volume increase [20, 21]. On further pressure release, the degree of rhombohedral distortion diminishes gradually, producing the mixture of Si-XII and Si-III or $bc8$ (body centered cubic structure with 8 atoms per unit cell), with the Si-XII persisting to ambient pressure [20, 21].

Two typical cyclic nanoindentation load-displacement curves of Si are presented in Figs. 1(a, b). A "pop-out" event, or sudden displacement discontinuity in the unloading curve [Fig. 1(a)], is often observed in the experiments at sufficiently high maximum loads (above ~ 20 mN for a Berkovich diamond indenter) and relatively slow unloading rates [22]. The respective "first unloading - reloading" internal loop in terms of average contact pressure vs. contact depth is shown in Fig. 1(c). Fig 1(e) shows a Raman spectrum from the same indentation. Clearly, the surface layer of the residual impression consists of the mixture of Si-III and Si-XII phases [Fig. 1(e)], which have similar vibrational properties and are difficult to separate in the Raman spectrum (see Ref. 23). We have recently shown [17] that such correlation between the load-displacement curves [Fig. 1(a)] and the phase composition of the indentation area [Fig. 1(e)] is not accidental; it is reproducible in more than 90% of cases. It is only natural to conclude that the

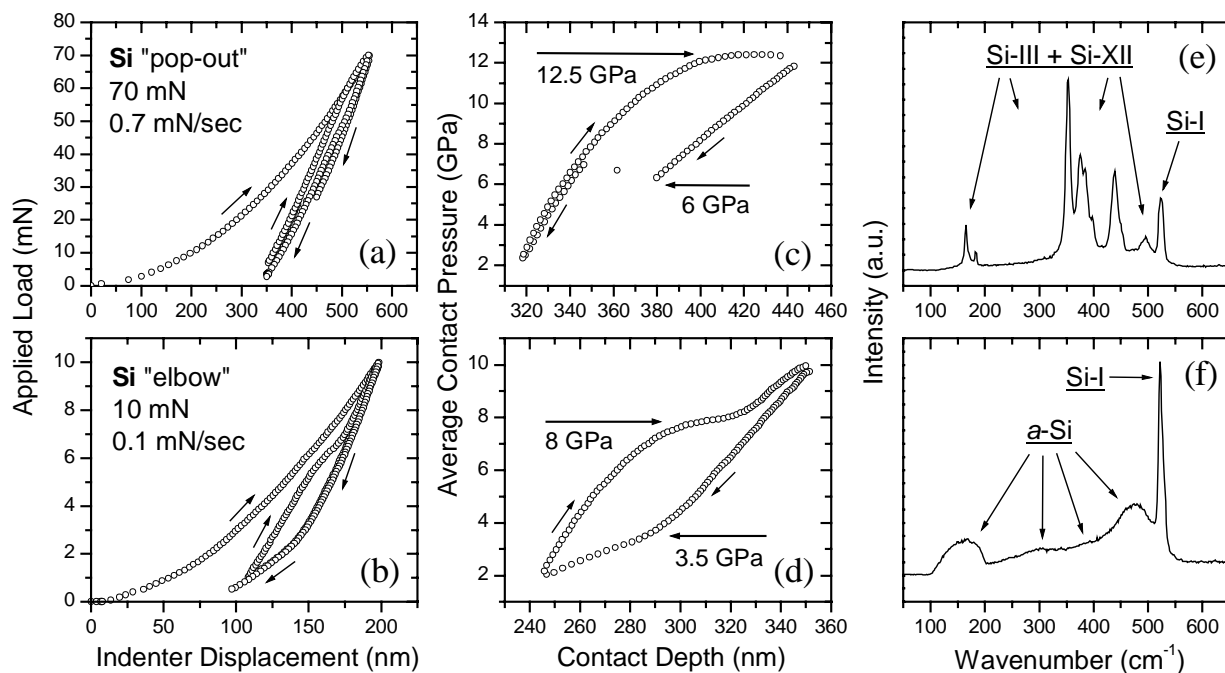


Figure 1. (a, b) Typical load-displacement curves in the nanoindentation of silicon. (c, d) Corresponding unloading and reloading average contact pressure vs. contact depth curves. (e, f) Raman spectra of the respective residual impressions.

Si-III and Si-XII phases have been formed in this case in the unloading stage from the metallic Si-II and that the pop-out event represents the instantaneous Si-II \rightarrow Si-XII transition.

The data in Fig. 1(c) may be thus regarded in the following manner. The elastic unloading of the metallic Si-II phase proceeds until its sudden transformation to Si-XII at 6 GPa. A relatively poor correlation with the pressures for Si-II \rightarrow Si-XII transformation measured in the high pressure cell experiments [20, 21] may be attributed to the presence of high shear stresses under a point-force indenter, which decrease the transformation pressure in accordance with Gilman's early predictions [5]. Further deformation of Si-XII is purely elastic as follows from the coincidence of the unloading and reloading curves. Upon reloading, Si-XII rapidly transforms back into Si-II at \sim 12.5 GPa. It should be noted that the phase transformation from Si-I to Si-II does not produce any step in the first loading curve; it is rather believed to occur during the whole loading stage when the point-force indenter is used. In contrast, in indentation with spherical indenters, the step in the loading curve ("pop-in") is indeed observed at pressures favorably correlating with the Si-I \rightarrow Si-II transition pressure given by pressurization experiments [4].

An "elbow", or gradual change in the slope of the unloading curve [Fig. 1(b)], is a completely reversible process (overlapping loops) and is often observed in the experiments either at low maximum loads (10 mN in this case) or at fast unloading. As revealed by Fig. 1(f), the elbow corresponds to the amorphous silicon in the residual impression; this result has also been shown to be reproducible and statistically significant [17]. In the case of elbow, we assume elastic unloading of Si-II until 3.5 GPa [Fig. 1(d)], when the gradual amorphization of Si-II begins. Upon subsequent reloading, the amorphous Si phase persists to 8 GPa, at which pressure it rapidly transforms to the metallic Si-II [Fig. 1(d)].

Similar to Si, Ge transforms from the semiconducting cubic diamond phase (Ge-I) into a metallic phase with β -tin structure (Ge-II) at about 10 GPa, with the mixture of Ge-I and Ge-II

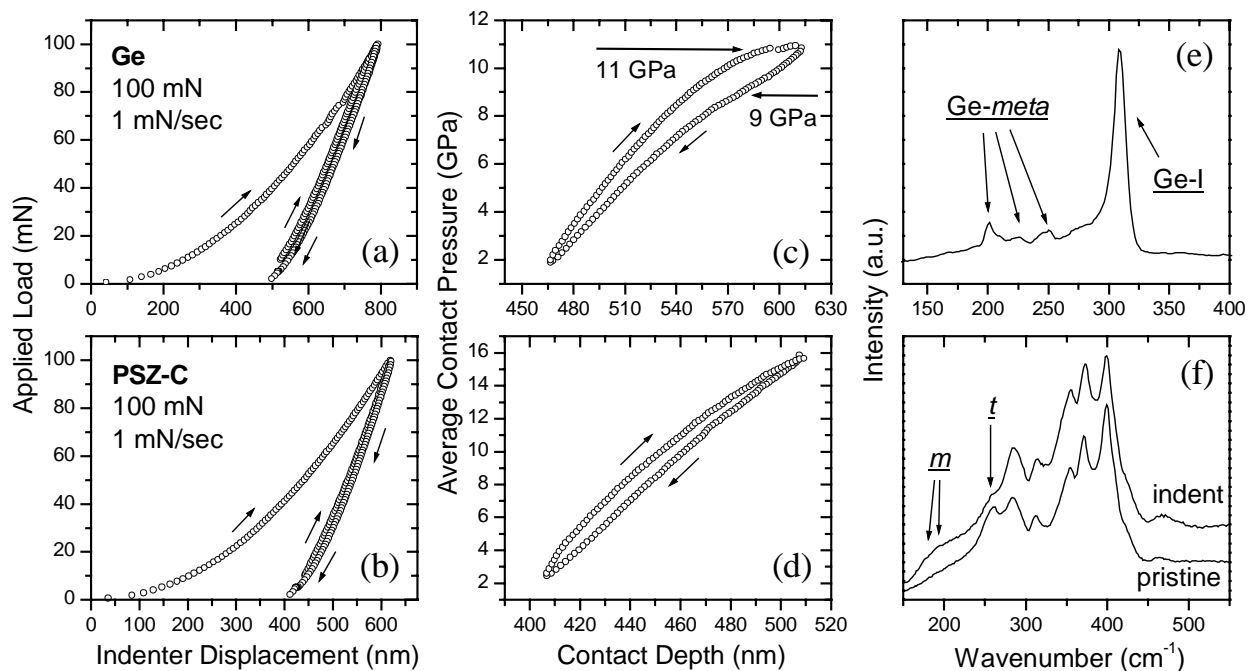


Figure 2. Typical load-displacement curves in the nanoindentation of (a) Ge and (b) PSZ-C. (c, d) Corresponding unloading and reloading average contact pressure vs. contact depth curves. (e, f) Raman spectra of the respective residual impressions.

persisting to higher pressures [24]. Upon decompression, transformation into a metastable Ge-III or *st12* phase (simple tetragonal structure with 12 atoms) is observed in most experiments at ~ 7.5 GPa [24], with its partial transformation to Ge-I at ambient conditions.

The typical load-displacement curves of Ge [Fig. 2(a)] hardly show any signs of phase transformations, unlike their Si counterparts [Figs. 1(a, b)]. However, examination of the internal unloading-reloading loop in terms of average contact pressure vs. contact depth curves [Fig. 2(c)] reveals deviations from the perfect elastic curve shape that can be attributed to the Ge-II \rightarrow Ge-III transition upon unloading (~ 9 GPa) and the subsequent reverse transformation (~ 11 GPa) on reloading. The rather broad and asymmetric hysteresis loop in Fig. 1(c) suggests gradual transformation that is not complete at the beginning of reloading. In support of this notion is the Raman spectrum in Fig. 2(e), which is typical for Ge samples obtained on pressure release from the metallic phase with 514.5 nm excitation; it apparently represents an unidentified Ge phase ("Ge-meta") that forms from Ge-III under laser irradiation at ambient conditions [23].

In zirconia-based ceramics, the tetragonal (*t*) phase is metastable at room temperature, and its spontaneous transformation to the monoclinic (*m*) phase is mainly inhibited by the lattice constrains to the associated volume expansion. Under an applied stress, however, the high activation energy for the *t* \rightarrow *m* transformation can be overcome, leading to the formation of monoclinic precipitates in the tetragonal matrix [25].

The load-displacement curves of PSZ-C shown in Fig. 2(b) are fairly featureless, with no visible signs of the *t* \rightarrow *m* transformation. However, the Raman spectra in Fig. 2(f) clearly show the decreased amount of the *t*-phase [26] within the indented area. A rather narrow hysteretic internal loop in Fig. 2(d) suggests that the transformation mostly occurs in the first loading stage, and only the remaining small amounts of the tetragonal phase are transformed into the monoclinic phase on reloading.

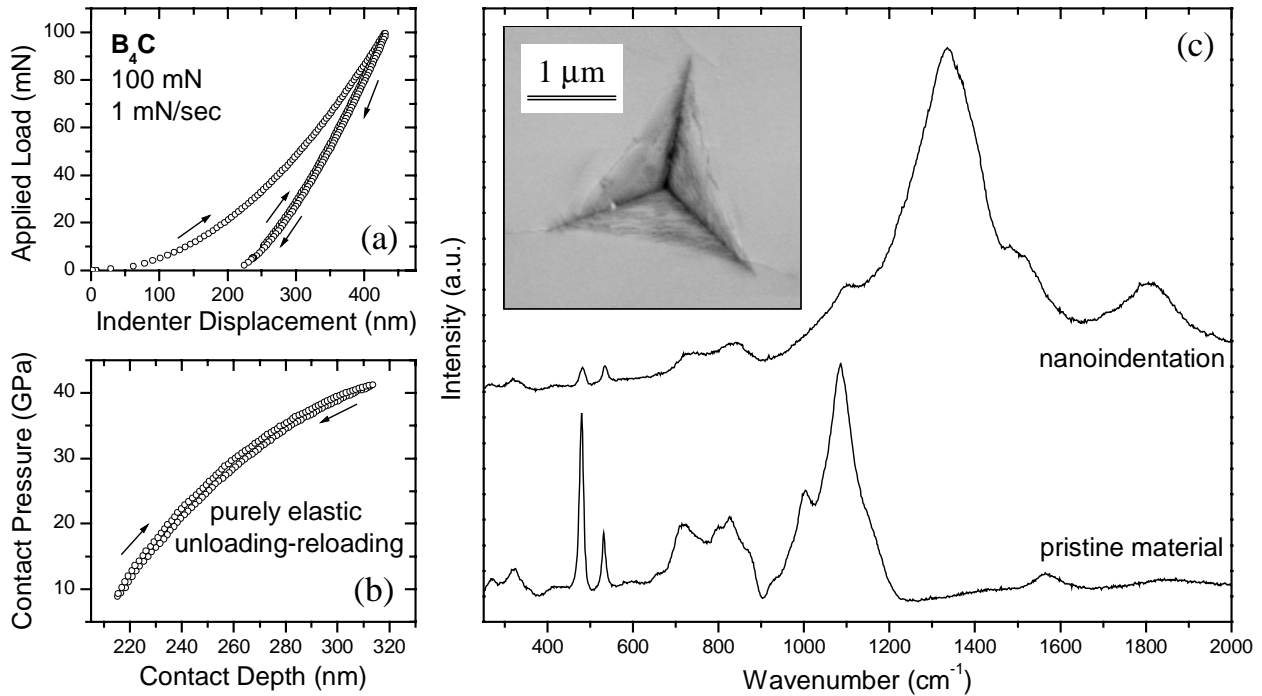


Figure 3. (a) Typical load-displacement curves in the nanoindentation of boron carbide. (b) Corresponding unloading and reloading average contact pressure vs. contact depth curves. (c) Raman spectra of the respective residual impression and the pristine material. Inset shows a scanning electron microscopy image of a 100 mN nanoindentation in $B_{4.3}C$.

Boron carbide is a member of a broad class of materials known as the boron-rich solids [27] and has a complicated hexagonal structure based on $B_{11}C$ icosahedra. Up to 11 GPa, no phase transformations of boron carbide have been observed [28], and we are not aware of any theoretical investigation of phase stability of boron carbide at elevated pressures. However, the nanoindentation hardness of boron carbide approaches 40 GPa, which implies that the high contact pressures during indentation may be capable of inducing structural changes in this material.

Both load-displacement [Fig. 3(a)] and average contact pressure-contact depth curves of $B_{4.3}C$ [Fig. 3(b)] show purely elastic unloading and subsequent reloading. This may be the case of a completely irreversible phase transition in the loading stage. Indeed, dramatic structural changes in the $B_{4.3}C$ single crystal under contact loading are revealed by Raman spectroscopy [Fig. 3(c)]. The Raman bands associated with numerous vibrational modes of the pristine boron carbide either disappear or are completely overwhelmed by a set of new high-frequency bands the most intense of which is at $\sim 1330\text{ cm}^{-1}$ [Fig. 3(c)]. Varying the laser wavelength rules out a possible assignment of these new high frequency bands to some sort of resonant scattering coupled with the excitation energy (fluorescence, *etc.*). However, additional characterization of the material in the vicinity of indentations by diffraction techniques will be required to definitely establish whether a new phase has been produced in nanoindentation of boron carbide.

CONCLUSIONS

The combination of the nanoindentation technique and Raman microanalysis provides evidence of phase transformations during contact loading in such materials as Si, Ge, and PSZ-C. For $B_{4.3}C$, the structural changes revealed by Raman spectroscopy are not supported by

nanoindentation data, possibly because the transformation is completely irreversible and is confined within the first loading stage. In general, any abrupt changes in the slope of the load-displacement curves may be a sign of possible phase transformation. Replotting of the nanoindentation data as average contact pressure vs. contact depth curves helps to reveal such changes and to estimate the corresponding transformation pressures.

ACKNOWLEDGEMENTS

The authors are thankful to Prof. George Gogotsi of the Institute for Problems of Strength (Kiev, Ukraine) for the PSZ-C sample and to Dr. Takaho Tanaka of the National Institute for Research in Inorganic Materials (Tsukuba, Japan) for the boron carbide sample. This research was supported by the National Science Foundation, Grant No. DMR-9874955.

REFERENCES

- [1] I. V. Gridneva, Y. V. Milman, and V. I. Trefilov, *Phys. Stat. Sol. (a)* **9**, 177 (1972).
- [2] D. R. Clarke, M. C. Kroll, P. D. Kirchner, R. F. Cook, and B. J. Hockey, *Phys. Rev.* **60**, 2156 (1988).
- [3] G. M. Pharr, W. C. Oliver, R. F. Cook, P. D. Kirchner, M. C. Kroll, T. R. Dinger, and D. R. Clarke, *J. Mater. Res.* **7**, 961 (1992).
- [4] E. R. Weppelmann, J. S. Field, and M. V. Swain, *J. Mater. Res.* **8**, 830 (1993).
- [5] J. J. Gilman, *Mat. Res. Soc. Symp. Proc.* **276**, 191 (1992).
- [6] M. C. Gupta and A. L. Ruoff, *J. Appl. Phys.* **51**, 1072 (1980).
- [7] D. L. Callahan and J. C. Morris, *J. Mater. Res.* **7**, 1614 (1992).
- [8] T. F. Page, W. C. Oliver, and C. J. McHargue, *J. Mater. Res.* **7**, 450 (1992).
- [9] T. Suzuki and T. Ohmura, *Philos. Mag. A* **74**, 1073 (1996).
- [10] Y. G. Gogotsi, A. Kailer, and K. G. Nickel, *Materials Research Innovations* **1**, 3 (1997).
- [11] A. Kailer, Y. G. Gogotsi, and K. G. Nickel, *J. Appl. Phys.* **81**, 3057 (1997).
- [12] Y. G. Gogotsi, A. Kailer, and K. G. Nickel, *J. Appl. Phys.* **84**, 1299 (1998).
- [13] A. Kailer, K. G. Nickel, and Y. G. Gogotsi, *J. Raman Spectrosc.* **30**, 939 (1999).
- [14] A. B. Mann, D. van Heerden, J. B. Pethica, and T. P. Weihs, *J. Mater. Res.* **15**, 1754 (2000).
- [15] J. E. Bradby, J. S. Williams, J. Wong-Leung, M. V. Swain, and P. Munroe, *Appl. Phys. Lett.* **77**, 3749 (2000).
- [16] Y. G. Gogotsi, V. Domnich, S. N. Dub, A. Kailer, and K. G. Nickel, *J. Mater. Res.* **15**, 871 (2000).
- [17] V. Domnich, Y. Gogotsi, and S. Dub, *Appl. Phys. Lett.* **76**, 2214 (2000).
- [18] N. V. Novikov, S. N. Dub, Y. V. Milman, I. V. Gridneva, and S. I. Chugunova, *Journal of Superhard Materials (Sverkhтвердые Materialy)* **18**, 32 (1996).
- [19] J. Z. Hu, L. D. Merkle, C. S. Menoni, and I. L. Spain, *Phys. Rev. B* **34**, 4679 (1986).
- [20] J. Crain, G. J. Ackland, J. R. Maclean, R. O. Piltz, P. D. Hatton, and G. S. Pawley, *Phys. Rev. B* **50**, 13043 (1994).
- [21] R. O. Piltz, J. R. Maclean, S. J. Clark, G. J. Ackland, P. D. Hatton, and J. Crain, *Phys. Rev. B* **52**, 4072 (1995).
- [22] G. M. Pharr, *Mat. Res. Soc. Symp. Proc.* **239**, 301 (1992).
- [23] H. Olijnyk and A. P. Jephcoat, *Phys. Stat. Sol. (b)* **211**, 413 (1999).
- [24] C. S. Menoni, J. Z. Hu, and I. L. Spain, *Phys. Rev. B* **34**, 362 (1986).
- [25] R. H. J. Hannink, P. M. Kelly, and B. C. Muddle, *J. Am. Ceram. Soc.* **83**, 461 (2000).
- [26] G. Morell, R. S. Katiyar, D. Torres, S. E. Paje, and J. Llopis, *J. Appl. Phys.* **81**, 2830 (1997).
- [27] J. L. Hoard and R. E. Hughes, in *The Chemistry of Boron and Its Compounds*, edited by E. L. Muetterties (Wiley, New York, 1967), p. 26.
- [28] R. J. Nelmes, J. S. Loveday, R. M. Wilson, W. G. Marshall, J. M. Besson, S. Klotz, G. Hamel, T. L. Aselage, and S. Hull, *Phys. Rev. Lett.* **74**, 2268 (1995).